

Microstructural and Electrical Properties of $(\text{WO}_3)_{1-x}(\text{MoO}_3)_x$ Thin Films Synthesized by Spray Pyrolysis Technique

Akl AA^{1,2*}, Aly SA¹ and Kaid MA¹

¹Physics Department, Faculty of Science, Minia University, El-Minia, Egypt

²Faculty of Science in Ad-Dawadmi, Physics Department, Shaqra University, KSA

Research Article

Received date: 29/09/2016

Accepted date: 30/10/2016

Published date: 07/11/2016

*For Correspondence

Akl AA, Faculty of Science in Ad-Dawadmi,
Physics Department, Shaqra University, KSA,
Tel: +2- 086-234868

Email: alaaakl2010@windowslive.com

Keywords: Mixed oxides, XRD, Spray pyrolysis,
Microstructural, Electrical properties, Thin films

ABSTRACT

New composite oxides of $(\text{WO}_3)_{1-x}(\text{MoO}_3)_x$ thin films were deposited by spray pyrolysis method. Microstructural and electrical properties of the films as-deposited and after annealing at different MoO_3 concentrations were investigated. XRD analysis, as-deposited films were amorphous, but after annealing, the crystallinity of WO_3 and MoO_3 were improved with a hexagonal structure with an increase in the MoO_3 , consisted of three non-stoichiometric phases, which have a monoclinic structure. Microstructure of a mixture based on the proportion of MoO_3 in the film. The electrical conductivity mechanisms appear to have two behaviors; extrinsic and intrinsic conductivities at lower and higher temperatures, respectively.

INTRODUCTION

Transition metal oxides have been widely used as gas-sensing, opto-electronic devices and inorganic electrochromic materials [1]. Tungsten trioxide (WO_3) and molybdenum oxide (MoO_3) thin film are one of the most promising material in Electrochromic and gas-sensing studies, and a common gasochromic window because their sensitivity to various gases, such as NO , NO_2 , CO , NH_3 and H_2 , which is due to the physical and chemical properties of these oxides [2-4]. The reason for choosing WO_3 as a doping with MoO_3 is because its film has a high transparency, high electrochemical activity and stability. The interaction between WO_3 and MoO_3 is unique due to their similar ionic radii and nearly-identical structures in their highest oxidation state. In addition, they were used in the electrochromic process as a cathode material due to the following reasons, they are (i) high specific energy density [5], (ii) undergo reversible potactic reaction with ions [6] and (iii) they have a higher electrochemical activity with the highest stability. In order to improve the quality of sensitivity of gas detection, the variation of gas-sensing and electrochromic devices, the binary combinations of oxides will modify and improve the characteristic of different oxides.

Composite trioxides of $(\text{WO}_3)_{1-x}(\text{MoO}_3)_x$ films have been prepared by different techniques; such as the vacuum evaporation [7,8], electro-deposition [9,10], sputtering [11], electron-beam deposition [12] and sol-gel deposition [13,14]. The spray pyrolysis process offers several advantages over conventional deposition techniques for the control of stoichiometry and film structure.

This work is aimed to present mixed metal oxide sprayed synthesis of new molybdenum trioxide doped tungsten trioxide film, WO_3 - MoO_3 and study the microstructural and electrical characteristics. The extent of a mixture concentration of MoO_3 ranges from 10-40 mol% in this study. A detailed structural characterization of the WO_3 - MoO_3 thin films was presented by X-ray diffraction (XRD) and as well as the study of the electrical properties was done. Also they have been studying the influence of thermal annealing on the properties of different concentrations. Structural and electrical properties correlation was aimed to study.

EXPERIMENTAL WORK

Samples Preparation

Molybdenum trioxide doped tungsten trioxide films were prepared using a chemical spray pyrolysis technique. The precursor solutions were prepared by dissolving ammonium paratungstate and ammonium paramolybdate with a solution molarity of 0.005 M in a hot distilled water of 333K. The molybdenum trioxide concentration is coincident with the percentage in atomic weight of ammonium paramolybdate dissolved in the sprayed solution. Different atomic percentages quantities, namely 10, 20, 30 and

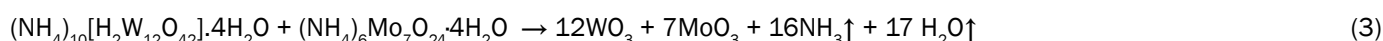
40 mol% were considered to get a composite of $(\text{WO}_3)_{1-x}(\text{MoO}_3)_x$ thin films. These solutions were mixed together accorded with atomic ratios to the deposition onto the heated glass substrate with change percentages referred to in **Table 1**. Equations expected the chemical reactions to get the compound as follows;

Table 1. The weights of the ammonium paratungstate and ammonium paramolybdate powder used in the preparation of samples for a mixture oxides of WO_3 and MoO_3 with different atomic percentage, which was dissolved in 100 ml of distilled water.

Ammonium paratungstate (gm)	Ammonium paramolybdate (gm)	Doping percentage (%)
1.400787	0.061795	10
1.245144	0.123590	20
1.089501	0.185385	30
0.933858	0.247180	40



The mixture of aqueous solution sprayed on the heated surface of glass substrate will be re-composed of WO_3 and MoO_3 which yield in the form of mixed $(\text{WO}_3)_{1-x}(\text{MoO}_3)_x$ thin films according to the following reaction equation;



The substrate temperature (T_{sub}) and film thickness were kept constant at 673K and 650 nm, respectively. The prepared samples of mixed WO_3 - MoO_3 were then annealed at temperature of 723K in the air for two hours. Thin films were carefully preserved in a desiccator to be used later in studying of their characterization. Films deposited on the glass substrates were used for structural and electrical characterization.

Stylus mechanical method was used for thickness measurements. In stylus instruments, a diamond needle of very small dimensions is used as the arm of an electromechanical pick-up. The position of the pickup is determined by a slider which is pressed on the area surrounding the needle to give the mean zero position.

Microstructural Characterization

X-ray diffraction (XRD) patterns were taken to collect by X-ray diffractometer (JEOL model JSDX- 60PA materials research), at room temperature using Ni-filtered Cu K_α radiation ($\lambda = 0.15418$ nm). Continuous scanning was applied with a slow scanning speed (1/min) and a small time constant (one second) for the two theta range from 4 to 80°. X-ray diffraction line profile analysis (XRD/LPA) was used to study the microstructure of the prepared samples. The line broadening is a result of the small size of the crystalline [15-18] as well as the non-uniform displacements strain of the atoms with respect to their reference lattice positions [18]. The observed integral breadth of the sample is a convolution of an instrument and a physical factor. This can be represented as follows;

$$I_{\text{obs}}(2\theta) = I_{\text{exp}}(2\theta) * I_{\text{s}}(2\theta) + \text{background} \quad (4)$$

where (*) is a convolution operator. The functions I_{obs} , I_{exp} and I_{s} are the broadening profiles of (i) the observed (B), (ii) the instrumental or standard sample (b) and (iii) the pure sample (β), noting that, these three broadening profiles are functions in the diffraction angle 2θ . The corrected Lorentzian (Cauchy) and Gaussian components of the integral breadth are given by

$$\beta_L = B - b \quad (5)$$

$$\beta_G^2 = B^2 - b^2 \quad (6)$$

where B and b are the broadening and instrumental factors, respectively. The average crystallite size (D) is calculated by using Scherrer's equation as follows [19];

$$D = K\lambda/\beta\cos\theta \quad (7)$$

Where the constant K is taken to be 0.94, λ the wavelength of X-ray used and β the broadening of pure specimen correction (full width at half maximum) of the diffraction peak. The internal micorstrain, $\langle \varepsilon \rangle$ in the film is calculated according to the relation;

$$\langle \varepsilon \rangle = \frac{\beta \cot \theta}{4} \quad (8)$$

Electrical Characterizations

Electrical resistivity measurements: The electrical resistance of the thin films was measured by using two-point probe technique. Two aluminum electrodes were deposited on the samples with leaving an uncoated trip in the middle of the film. Load-spring was fixed to two copper rods used for better contact with the two aluminum electrodes. The resistance of the sample was measured using a digital Keithly electrometer (model 616) and a stabilized power supply. The temperature of the specimen was recorded with chromel alumel in close thermal contact with the specimen surface. The temperature dependence of d.c. electrical

resistivity, ρ_{dc} for the film was measured in the temperature range from 300 to 523K. It was calculated by;

$$\rho_{dc} = \frac{R w t}{d} \tag{9}$$

where d is the distance between two copper electrodes (1.4 cm), R is the resistance of thin film (Ω), w is the electrode length covered by the film (width of the thin film is 2.5 cm) and t is the film thickness (cm).

Sheet resistance measurement: The sheet resistance of semiconductor is considered as a widely used technique to characterize the thin films. It measures the resistance of thin films across a square area to identify the nature of the roughness of film surface and thickness homogeneity. To calculate the sheet resistance of thin films is implied that the current passes through the sheet plane and is not perpendicular to it. Also, the resistivity of bulk material, ρ can be calculated by multiplying the film thickness, t and the sheet resistance R_{sh} as given by the following formula [20];

$$\rho = R_{sh} . t \tag{10}$$

RESULTS AND DISCUSSION

Structural Characteristics

The structure of as-synthesized of composite WO_3 - MoO_3 thin films: XRD patterns of the as-deposited samples as well as samples of a composite $(WO_3)_{1-x}(MoO_3)_x$ films with different concentrations of MoO_3 are shown in Figure 1. Results showed that, the investigated samples of tungsten and molybdenum trioxide have a polycrystalline structure. All the diffraction peaks of pre-annealed WO_3 in the lower diffraction pattern can be indexed to the hexagonal structure of WO_3 with lattice constants of $a=b=0.73025$ nm, $c=0.38970$ nm, $\alpha=\beta=90^\circ$, $\gamma=120^\circ$ (PDF card, 75-2187). No peaks of any other phase or impurities were observed in the XRD patterns. Also, the second diffraction pattern is perfectly with the MoO_3 , which have a hexagonal structure (PDF card, 05-0508). When the MoO_3 mixed with WO_3 , all the diffraction patterns completely amorphous form of all doped concentrations. This is may be due to, the properties of composites of oxide materials depend not only on the chemical and physical nature of of each compound, but also on the interface and synergy between them.

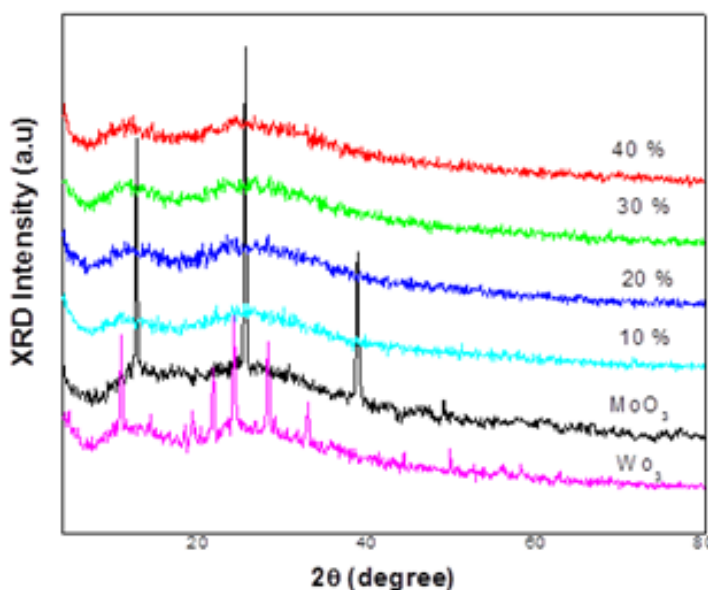


Figure 1: XRD patterns of as-deposited of a mixed MoO_3 and WO_3 thin films.

The effect of annealing on the structure of WO_3 - MoO_3 thin films: The change of crystallinity and structural identification after thermal annealing of WO_3 thin films with the different concentration of MoO_3 were studied by using XRD technique [21-23]. The diffractograms of the thin films after annealing at temperature 723K for two hours using XRD are shown in **Figure 2**. All the investigated samples were transformed into a polycrystalline structure. The strong and sharp diffraction peaks also indicate a good crystallinity of the samples. Compositions and phase identification process of the samples were recorded in **Tables 2 and 3**. It can be revealed that, the three non-stoichiometric phases Mo - W - O_3 , $Mo_{9.35}W_{1.65}O_{32}$ and $W_{0.71}Mo_{0.29}O_3$ are present. The phases are depending on the doping concentration. At concentration of 10mol%, the peaks expected corresponding to the a hexagonal structure as well as for un-doped WO_3 [24]. The characteristic diffraction lines corresponding to (100), (110), (111), and (200) planes of WO_3 was observed and coincides with PDF number 75-2187. However, at higher concentrations of 20% and 30%, the composition of the films has a monoclinic structure with characteristic lines corresponding to (201), (010) and (411) planes of $Mo_{9.35}W_{1.65}O_{32}$. This is matched with the planes of PDF 73-2198. Furthermore, the composition of the

films at higher concentration of MoO_3 (40%) has a monoclinic structure with lines (111), (200) and (112) planes of $\text{W}_{0.71}\text{Mo}_{0.29}\text{O}_3$ which coincide with the planes of PDF 76-1279 [25,26].

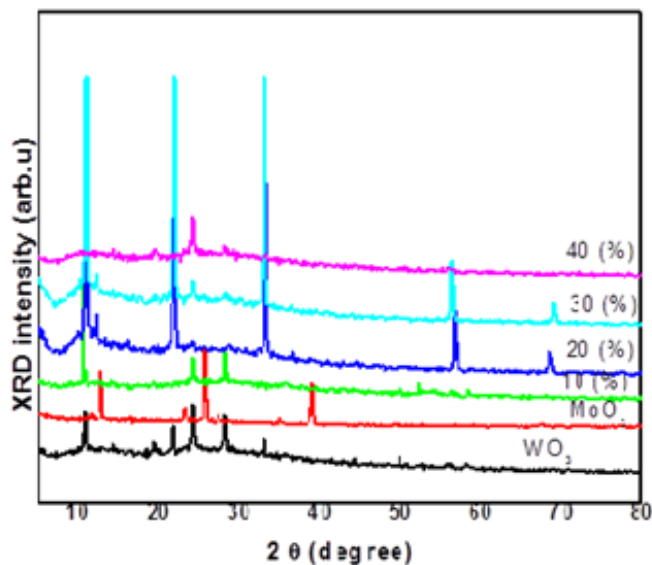


Figure 2. XRD patterns of a mixed MoO_3 and WO_3 films with different doping percentages after annealing at 723K for two hours.

The chemical reaction mechanism of the composite W-Mo-O_3 can be explained according to electrochemical activity series of elements W and Mo, where WO_3 and MoO_3 have a hexagonal structure. It was found that, the excess of Mo content increases the unit cell volume of the formed $\text{WO}_3\text{-MoO}_3$ network. The structure of composite W-Mo-O_3 alloys was found to be a non-stoichiometric phase of $\text{Mo}_{9.35}\text{W}_{1.65}\text{O}_{32}$ which has a monoclinic structure in the concentration range 10 to 30% of MoO_3 . The observed three peaks at Bragg's angles are $2\theta=11.00$, 21.90 and 33.00° and corresponding the Millar indices are (201), (010) and (411). XRD data reveal that the composite system of W-Mo-O_3 phase becomes no stable and its formation is independent of MoO_3 concentration. This result indicates that the stoichiometric ratio is verified [27,28].

The effect of annealing on the crystallite size and internal microstrain: The variation of crystallite/domain size with varying doping percentage is shown in Figure 3. It is observed that, the crystallite size has nearly the same value up to a concentration of 30%, while at a concentration value of 40%, the crystallite size was suddenly increased. This is due to, the composite of WO_3 and MoO_3 are the same of atomic volume. So the rate of agglomeration growth of thin films is kept constant. But at higher concentration of MoO_3 , the rate of growth was increased. These values of crystallite size are in good agreement with the data estimated by Kowar et al. for a similar phase and prepared by spray pyrolysis technique and other techniques [29-31].

The effect of doping percentage on the internal microstrain is depicted in **Figure 4**. It can be seen that, the internal microstrain depending on the MoO_3 concentration. Since the internal microstrain is equivalent to variations in the d-spacing within domains by an amount depending on the elastic constants of the material and the nature of internal stresses. This is due to, the growth of MoO_3 inserted the host unit cell of WO_3 , consequently the inter planer spacing was shifted. This shift in the plane position or the internal microstrain is produced as a result of the growth process of the samples and the preparation conditions. Note from the **Figure 4**, the value of internal microstrain nearly the same value at MoO_3 concentrations of 10 to 30%, while suddenly increased when the concentration 40%. It is expected that the addition of more MoO_3 causes imperfections to the original lattice of WO_3 and thus increases the amount of internal stress, which in turn increases the amount of internal microstrain. This confirms that, the WO_3 phase has a good crystallinity formation in the studied range from 0 to 30% [32].

Electrical Properties of $\text{WO}_3\text{-MoO}_3$ Thin Films

The resistivity of semiconductor depends on several parameters, e.g. impurity concentrations, crystal defect concentration, temperature (lattice vibrations and phonon), and electron-hole concentrations. The electrical characterization of the as deposited $\text{WO}_3\text{-MoO}_3$ thin films at different doping concentrations of 0%, 10%, 20%, 30% and 40 mol% was carried out by means of the resistivity-temperature measurements.

Effect of temperature on electrical resistivity: The electrical resistivity of mixed $\text{WO}_3\text{-MoO}_3$ thin films as a function of temperature according to the Pertritz model. The thermal activation energies, ΔE , were calculated by using the following relation [33],

$$\rho_{dc} = \rho_o \exp\left(\frac{\Delta E_a}{K_B T}\right) + \rho_1 \exp\left(\frac{\Delta E_{a1}}{K_B T}\right) \tag{11}$$

Where ρ_o and ρ_1 are pre-exponential constants, K_B the Boltzmann constant and T is the absolute temperature. **Figure 5** shows the representation of the $\ln\rho_{dc}$ and the reciprocal absolute temperature ($1000/T$). It is clear that, the electrical resistivity exponentially decreased with increasing temperature for all samples regardless of the doping concentration. Furthermore, the electrical resistivity is found to be strongly dependent on the composition of thin films. This is explained by increasing of the number of thermally excited electrons [33,34].

On the other hand, the dark electrical resistivity (ρ_{dc}), for temperature at three different zones for WO_3 - MoO_3 thin films was

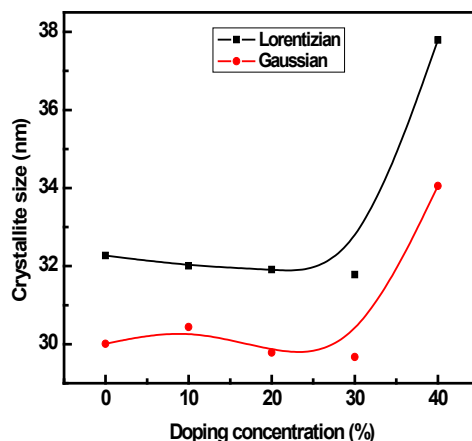


Figure 3: The estimated crystallite size of a mixed MoO_3 and WO_3 films as a function of MoO_3 contents.

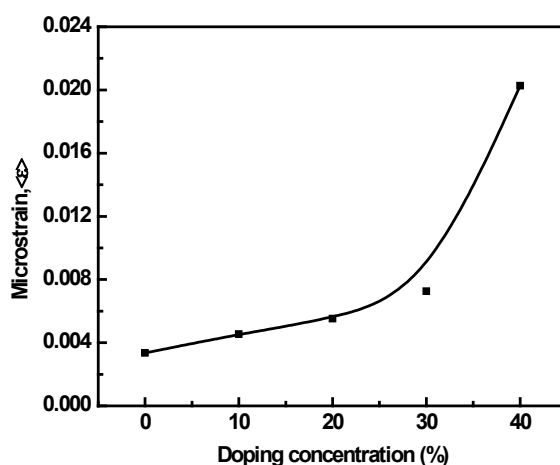


Figure 4. The microstrain as a function of MoO_3 concentration.

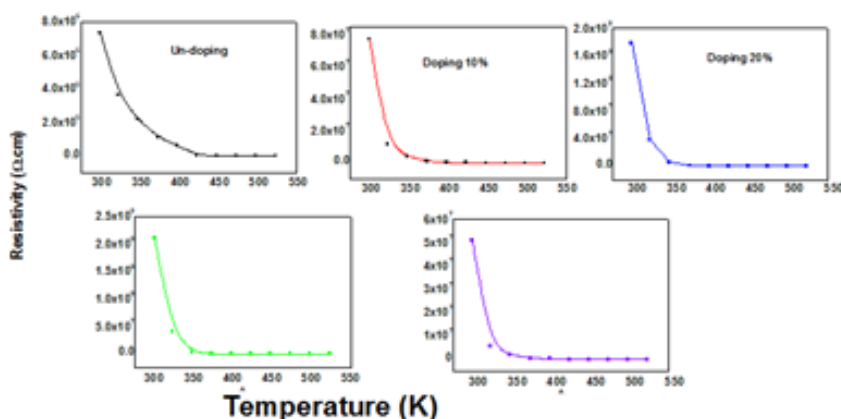


Figure 5.The electrical resistivity versus temperature at different MoO_3 percentages.

Table 2: X-ray diffraction results of thin films sprayed from pure trioxides of tungsten and molybdenum, as well as from different ratios of a mixture of MoO₃ and WO₃ after thermal annealing at a temperature of 723K for two hours.

2θ	WO ₃ -Pure		MoO ₃ -Pure		10% MoO ₃		20% MoO ₃		30% MoO ₃		40% MoO ₃	
	d(Å)	(hkl) Phase	d(Å)	(hkl) Phase	d(Å)	(hkl) Phase	d(Å)	(hkl) Phase	d(Å)	(hkl) Phase	d(Å)	(hkl) Phase
10.00					8.85	(100) W _{0.71} Mo _{0.29} O ₃	8.85	(100) W _{0.71} Mo _{0.29} O ₃				
10.94	8.08	(100) WO ₃			8.04	(201) Mo-W-O ₃	8.04	(201) Mo-W-O ₃	8.04	(201) Mo-W-O ₃		
12.18					7.38	(201) Mo _{9.35} W _{1.65} O ₃₂	7.38	(201) Mo _{9.35} W _{1.65} O ₃₂				
13.13			6.74	(020) MoO ₃								
14.38	6.26	(100) WO ₃			6.28	(111) W-Mo-O ₃	6.28	(111) W-Mo-O ₃			6.28	(111) W-Mo-O ₃
16.25					5.45	(001) W _{0.71} Mo _{0.29} O ₃	5.45	(001) W _{0.71} Mo _{0.29} O ₃				
19.38	4.58	(001) WO ₂			4.58	(010) Mo _{9.35} W _{1.65} O ₃₂	4.58	(010) Mo _{9.35} W _{1.65} O ₃₂	4.58	(010) Mo _{9.35} W _{1.65} O ₃₂	4.58	(010) Mo _{9.35} W _{1.65} O ₃₂
21.56	4.12	(011) WO ₃			4.06	(010) Mo-W-O ₃	4.06	(010) Mo-W-O ₃	4.06	(010) Mo-W-O ₃		
23.13			3.85	(110) MoO ₃								
24.22	3.67	(110) WO ₃			3.68	(111) W _{0.71} Mo _{0.29} O ₃	3.68	(111) W _{0.71} Mo _{0.29} O ₃	3.68	(111) W _{0.71} Mo _{0.29} O ₃	3.68	(111) W _{0.71} Mo _{0.29} O ₃
25.63			3.48	(040) MoO ₃								
27.50			3.24	(021) MoO ₃								
28.13	3.17	(200) WO ₃			3.18	(200) W _{0.71} Mo _{0.29} O ₃	3.18	(200) W _{0.71} Mo _{0.29} O ₃	3.18	(200) W _{0.71} Mo _{0.29} O ₃	3.18	(200) W _{0.71} Mo _{0.29} O ₃
29.22			3.05	(130) MoO ₃								
30.46					2.93	(200) Mo _{9.35} W _{1.65} O ₃₂	2.93	(200) Mo _{9.35} W _{1.65} O ₃₂				
32.81					2.73	(411) Mo-W-O ₃						
34.38	2.61	(111) WO ₃			2.48	(201) W _{0.71} Mo _{0.29} O ₃	2.48	(201) W _{0.71} Mo _{0.29} O ₃	2.48	(201) W _{0.71} Mo _{0.29} O ₃		
36.25			2.31	(060) MoO ₃								
39.06					2.09	(300) W _{0.71} Mo _{0.29} O ₃	2.09	(300) W _{0.71} Mo _{0.29} O ₃				
43.28												
44.37	2.04	(002) WO ₃										
50.00	1.82	(220) WO ₃			1.82	(220) W _{0.71} Mo _{0.29} O ₃	1.82	(220) W _{0.71} Mo _{0.29} O ₃				
52.50					1.74	(112) W-Mo-O ₃	1.74	(112) W-Mo-O ₃			1.74	(112) W-Mo-O ₃
56.25												
56.72					1.62	(221) Mo _{9.35} W _{1.65} O ₃₂	1.62	(221) Mo _{9.35} W _{1.65} O ₃₂	1.64	(202) Mo _{9.35} W _{1.65} O ₃₂		
58.13	1.59	(311) WO ₃			1.60	(202) W _{0.71} Mo _{0.29} O ₃	1.60	(202) W _{0.71} Mo _{0.29} O ₃				
67.50			1.39	(010) MoO ₃								
68.75					1.60	(112) W _{0.71} Mo _{0.29} O ₃	1.60	(112) W _{0.71} Mo _{0.29} O ₃				
69.22					1.35	(411) Mo _{9.35} W _{1.65} O ₃₂	1.35	(411) Mo _{9.35} W _{1.65} O ₃₂	1.35	(411) Mo _{9.35} W _{1.65} O ₃₂		

recorded in **Table 3**. It is observed that, the electrical resistivity is changed randomly with the doping percentages of MoO₃. But generally, a significant increase in the resistivity is observed at any MoO₃ concentration reaches a higher value at a concentration of 30% and then returning to decrease again at a concentration 40%. Where the electrical resistivity of the compound (WO₃)_{1-x}(MoO₃)_x does not take a certain behavior, due to the non-stoichiometric phase formation of the film as a result of increasing impurities (Mo atoms).

Table 3. The electrical resistivity and sheet resistance at three different temperature zones with different doping concentrations.

Doping percentage mol (%)	300K		400K		523K	
	$\rho(\Omega.cm)$	$R_{sh}(\Omega/\square)$	$\rho(\Omega.cm)$	$R_{sh}(\Omega/\square)$	$\rho(\Omega.cm)$	$R_{sh}(\Omega/\square)$
0	7.33×10^6	1.13×10^{11}	6.26×10^5	9.63×10^9	3.53×10^2	5.43×10^6
10	7.75×10^7	1.19×10^{12}	1.34×10^5	2.06×10^9	2.90×10^3	4.46×10^7
20	1.79×10^8	2.75×10^{12}	2.06×10^5	3.17×10^9	3.86×10^2	5.94×10^6
30	2.11×10^8	3.25×10^{12}	8.11×10^4	1.25×10^9	3.36×10^2	5.17×10^6
40	5.12×10^7	7.88×10^{11}	1.28×10^5	1.97×10^9	2.45×10^2	3.77×10^6

Effect of temperature on sheet resistance: The sheet resistance of doping semiconductor is considered a widely used technique to characterize the thin films. It measures the resistance of thin films across a square area to identify the nature of the roughness of film surface and thickness homogeneity. Measurements of electrical sheet resistance, R_{sh} of the WO₃ mixed with MoO₃ thin films were carried out in the temperature range 300-523K, as shown in **Figure 6**. It is observed that, the sheet resistance for all ratios of MoO₃ additives is the exponential decreasing behavior as a function of temperature. Also, its value of R_{sh} does not only depend on the ratio of adding MoO₃, but also depends on the morphology of the film surface. Furthermore, the sheet resistance, R_{sh} values at temperatures in three different zones for mixed thin films of (WO₃)_{1-x}(MoO₃)_x was listed in **Table 3**. It was observed that, the sheet resistance decreased with increasing MoO₃ concentration. The decreases in R_{sh} may be due to substitution of Mo-atoms instead of the W-atoms in the unit cell, which causes a decrease of energy gap consequently leads to the increase of electrical conductivity.

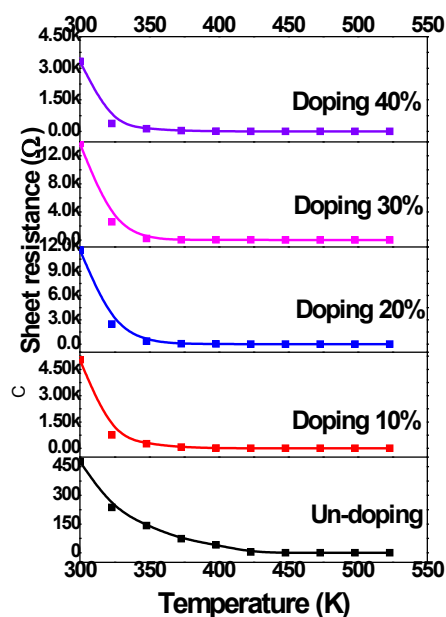


Figure 6: The sheet resistance versus temperature at different MoO₃ concentrations.

Conductivity mechanisms and activation energy: The representation of logarithmic resistivity, $\ln \rho_{dc}$ versus the reciprocal absolute temperature ($1000/T$) with the different doping percentage is shown in **Figure 7**. It is clear that, the two different linear regions and their dependence upon the selected temperature range. The first region is identified at low temperature (LT). This region extends also upwards as far as the impurity exhaustion temperatures and is identified as an extrinsic conductivity of semiconductor due to the ionization of impurity atoms. At the low temperature range, the data followed Pertritz expression indicated that the conduction attributed to the thermally assisted hopping of carriers between localized states closes to the Fermi level [34,35]. The second region (higher temperature region, HT) is identified with the intrinsic conduction of semiconductor. Within this region, the density of carriers is equal to that of intrinsic carriers [31]. This can be explained due to the lower degree of crystallinity and the small crystallite size. Also, the presence of defects such as structural disorders, dislocations and surface imperfections also play an essential role in decreasing the conductivity as reported earlier [31]. As, the transition here depends on two parameters; the temperature and lattice vibrations which create phonons, will produce electron-phonon interaction. This interaction causes hindering for electrons, so electrons need more energy to be activated. This interprets the increasing of activation energy values

of the second region [34]. The corresponding activation energies of the two regions were listed in **Table 4**. It is observed that, the obtained activation energy in the lattice vibration region (HT) is approximately equal to one half of the optical energy gap [36,37]. Also, ΔE values for all of WO_3 mixed with MoO_3 thin films indicate that the prepared samples were semiconductors materials. On the other hand, our all present data were consonant with the results of the other semiconducting materials [34,37-39].

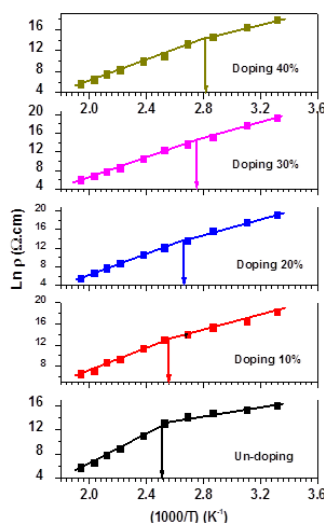


Figure 7: $\ln \rho$ versus $(1000/T)$ at different MoO_3 percentages.

The change in the transition temperature (T_c) in conductivity mechanism as a function of MoO_3 concentration is represented in **Figure 8** and has been recorded in **Table 4**. Represented measured data was fitted to be obtained straight lines satisfying of the following equation [31,36];

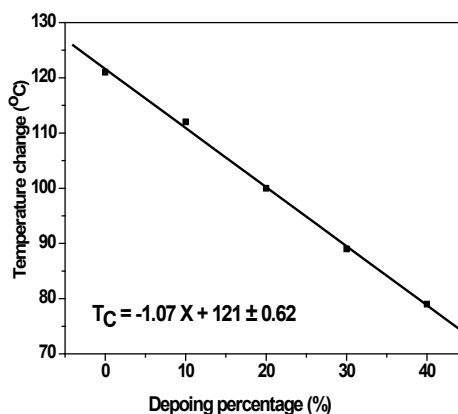


Figure 8. The transition temperature of conductivity mechanism versus MoO_3 percentage.

$$T_c = -1.07 X + 121 \pm 0.62 \tag{12}$$

These results can be interpreted as follows, since the Mo atom is an inserted within the host unit cell of WO_3 instead of the W atom because the size of Mo atom is equal to the size of W atom. So the dimensions of the unit cell are remaining constant in the three directions for the same extension. So, the shift of transition temperature, T_c is due to increase in the doping percentage, which represent the impurities in the composite where the conductivity mechanism depends on the temperature, impurities and crystal defects. Therefore, the shift in T_c can be attributed to the change in the impurity content which is affecting the conductivity mechanism.

Table 4: The residual resistivity, activation energy and the temperature change of conductivity mechanisms with different MoO_3 doping percentage.

Doping mol (%)	T_c		$\rho_o(\Omega.cm)$	$E_{a1}(eV)$	$\rho_{o1}(\Omega.cm)$	$E_{a2}(eV)$
	$10^3/T$	$T(^{\circ}C)$				
Un-doping	2.54	121	73.13×10^3	0.3389	24.53	0.9306
10%	2.60	112	7.33×10^3	0.5511	99.48	0.9703
20%	2.68	100	7.35×10^2	0.7547	44.70	0.9409
30%	2,76	89	4.93×10^2	0.8315	54.59	0.8987
40%	2.84	79	1.34×10^3	0.6469	54.59	0.8461

CONCLUSIONS

1. Composite trioxide $(\text{WO}_3)_{1-x}(\text{MoO}_3)_x$ thin films were deposited on the previous glass heating substrates by using the spray pyrolysis technique.
2. The thermal annealing process in the air at 723 K for two hours was done.
3. XRD reveals that, composite W-Mo-O₃ alloys were found to be non-stoichiometries phases of Mo-W-O₃, $\text{Mo}_{9.35}\text{W}_{1.65}\text{O}_{32}$ and $\text{W}_{0.71}\text{Mo}_{0.29}\text{O}_3$ which have a monoclinic structure.
4. The microstructure (crystallite size and internal microstrain) was estimated as a function of MoO₃ content.
5. The electrical properties (resistivity, sheet resistance and activation energies) of a composite $(\text{WO}_3)_{1-x}(\text{MoO}_3)_x$ were carried out.
6. The conductivity mechanisms divided into the two processes; an extrinsic conductivity and intrinsic conduction.
7. Transition temperature of the conductivity mechanism was increased with MoO₃ concentrations.

REFERENCES

1. Arveez Ahmed HM and Begum NS. Synthesis and characterization of MoO-WO composite thin films by liquid phase deposition technique: Investigation of its photochromic properties. Bull Matter Sci 2013; 36: 45-49.
2. Bathe SR and Patil PS. Electrochromic characteristics of fibrous reticulated WO₃ thin films prepared by pulsed spray pyrolysis technique. Sol Energy Mater Sol Cells 2007; 91: 1097-1101.
3. Patil RS, et al. Structural and optical properties of electrodeposited molybdenum oxide thin films. Appl Surf Sci 2006; 252: 8050-8056.
4. Patil PR and Patil PS. Preparation of mixed oxide MoO₃ WO₃ thin films by spray pyrolysis technique and their characterization. Thin Solid Films 2001; 382: 13-22.
5. Meenakshi M, et al. Optical dispersion characterization of NiO thin films prepared by nebulized spray technique. Int J Chem Tech Res 2014; 6: 5196-5202.
6. Sberveglieri G, et al. WO₃ sputtered thin films for NO_x monitoring. Actuators B: Chem 1995; 26-27: 89-92.
7. Ferroni M, et al. Characterization of a molybdenum oxide sputtered thin film as a gas sensor. Thin Solid Films 1997; 307: 148-151.
8. Ferroni M, et al. MoO₃-based sputtered thin films for fast NO₂ detection. Actuators B: Chem 1998; 48: 285-288.
9. Hiruta Y, et al. Absorption Bands of Electrochemically-Colored Films of WO₃, MoO₃ and Mo_cW_{1-c}O₃. Jpn J Appl Phys 1984; 23: 1624.
10. Yamada S, et al. Infrared Absorption of Colored and Bleached Films of Tungsten Oxide. Solid State Ionics 1990; 40: 487-490.
11. Monk PMS and Chester SL. Electrodeposition of Films of Electrochromic Tungsten-Oxide Containing Additional Metal-Oxides. Electrochim Acta 1993; 38: 1521-1526.
12. Monk PMS, et al. Electrochromic tungsten oxide: doping with two or three other metal oxides. J Mater Chem 1994; 4: 1071-1074.
13. Nguyen MT and Dao LH. Poly(N-benzylaniline)/(poly(AMPS)/WO₃ solid-state electrochromic cell. J Electrochem Soc 1989; 136: 2131-2132.
14. Pennisi A, et al. Electrochromic properties of tungsten- molybdenum oxide electrodes. Solar Energy Mater Solar Cells 1992; 28: 233-247.
15. Abouhilou F, et al. X-ray peak profile analysis of dislocation type, density and crystallite size distribution in cold deformed Pb-Ca-Sn alloys. Trans Nonferrous Met Soc China 2012; 22: 604-607.
16. Mukherjee P, et al. Microstructural changes in oxygen-irradiated zirconium-based alloy characterised by X-ray diffraction techniques. Mater Characterization 2005; 55: 412.
17. Vives S, et al. X-ray diffraction line profile analysis of iron ball milled powders. Mater Sci Eng A 2004; 366: 229-238.
18. Snyder RL. Analytical profile fitting of X-ray powder diffraction profiles in Rietveld analysis. In: The Rietveld method. [Edn]. Young RA. International Union of Crystallography and Oxford University Press, New York 111-131.

19. Cullity BD. Elements of X-ray diffraction, [2nd edn] Addison-Wesley, California, USA 1978; 102.
20. Ozer N and Lampert CM. Thin Solid Films 1999; 349: 205.
21. Patil CE, et al. Electrochromic performance of the mixed V_2O_5 - WO_3 thin films synthesized by pulsed spray pyrolysis technique. Curr Appl Phys 2014; 14: 389.
22. Patil CE, et al. Electrochromic performance of mixed V_2O_5 - WO_3 thin films synthesized by pulsed spray pyrolysis technique. Mater Chem Phys 2011; 126: 711-716.
23. Debecker DP, et al. Total oxidation of benzene and chlorobenzene with MoO_3 - and WO_3 -promoted V_2O_5/TiO_2 catalysts prepared by a nonhydrolytic sol-gel route. Catal Today 2010; 157: 125-130.
24. Phillips J. Evaluation of the fundamental properties of quantum dot infrared detectors. J Appl Phys 2002; 91: 4590-4594.
25. McCarthy TJ and Kanatids MG. Synthesis in Molten Alkali Metal Polyselenophosphate Fluxes: A New Family of Transition Metal Selenophosphate Compounds, $A_2MP_2Se_6$ (A=K, Rb, Cs; M=Mn, Fe) and $A_2M'2P_2Se_6$ (A=K, Cs; M'=Cu, Ag). Inorg Chem 1995; 34: 1257-1267.
26. Ozer N and Lampert CM. Electrochromic performance of sol-gel deposited WO_3 - V_2O_5 . Thin Solid Films 1999; 349: 205.
27. Yang Y, et al. High Capacity and Contrast of Electrochromic Tungsten-Doped Vanadium Oxide Films. Solid State Ionics 2008; 179: 1250-1255.
28. Akl AA, et al. Characterization of tungsten oxide films of different crystallinity prepared by RF sputtering. Physica B 2003; 325: 65-75.
29. Patil PS, et al. Thickness-dependent properties of sprayed iridium oxide thin films. Mater Chem Phys 2003; 80: 667-675.
30. Kawar RK, et al. Substrate temperature dependent structural, optical and electrical properties of spray deposited iridium oxide thin films. Appl Surf Sci 2003; 206: 90-101.
31. Shahane GS and Deshmukh LP. Structural and electrical transport properties of CdS 0.9 Se 0.1: in thin films: effect of film thickness. Mat Chem Phys 2001; 70: 112-116.
32. Stamate MD. On the dielectric properties of dc magnetron TiO_2 thin films. Appl Surf Sci 2003; 218: 317.
33. McPedran RC, et al. Unambiguous determination of optical constants of absorbing films by reflectance and transmittance measurements. Appl Opt 1984; 23: 1197.
34. Pertriz RL. Theory of Photoconductivity in Semiconductor Films. Phys Rev 1956; 104: 1508.
35. Stamate M. On the dielectric properties of dc magnetron TiO_2 thin films. PhD Thesis, Al.I.Cuza University, Iasi, Romania 1999.
36. Tanaka K. Optical Properties and Photoinduced Changes in Amorphous As-S Films. Thin Solid Films 1980; 66: 271-279.
37. Hwakim S and Hwangbo CK. Influence of Ar ion-beam assistance and annealing temperatures on properties of TiO_2 thin films deposited by reactive DC magnetron sputtering. Thin Solid Films, 2005; 475: 155-159.
38. Seoudi R, et al. Synthesis, characterization, and electrical properties studies of cadmium selenide nanoparticle. Physica B 2008; 403: 152-158.
39. Fayek SA, et al. Electrical conductivity of amorphous semiconducting films of system $(Ge_{20}As_{30}Se_{50-x}Te_x)$. Solid State Com 1995; 93: 213-217.